RECENT STAINLESS STEEL RESEARCH IN THE UK: AN IMPROVED METHOD FOR STRUCTURAL DESIGN AND NUMERICAL MODELLING

L Gardner
Imperial College London

B A Burgan
The Steel Construction Institute

Abstract

This paper reports on recently conducted structural stainless steel research in the UK and summarises the activities and findings of two major projects. The first concerns the development of a new approach to structural stainless steel design that is based on exploiting the full deformation capacity of cross-sections, by adopting a continuous method of cross-section classification and member design, coupled with more accurate material modelling. The second involves the numerical modelling of high-strength cold-worked stainless steel conducted as part of the ECSC funded project 'Structural design of cold-worked austenitic stainless steel'.

1 INTRODUCTION

Stainless steel is commonly regarded as an extravagant solution to structural engineering problems. Changing attitudes within the construction industry and a global transition towards sustainable development and reduction in environmental impact are sure to bring increased interest in the use of stainless steel. Nonetheless the need to improve the efficiency of structural stainless steel design guidance and to develop the availability and diversity of the current product range is clear. This paper relates directly to this challenge by describing a new proposed approach to stainless steel structural design and by presenting results from a numerical study on high-strength cold-formed stainless steel.

2 A NEW APPROACH TO STRUCTURAL STAINLESS STEEL DESIGN

2.1 Background

The past fifteen years have seen the introduction or major revision of structural stainless steel design codes throughout the world, and at the same time, interest in the use of stainless steel in construction has been accelerating. However, stainless steel is still viewed as an extravagant solution to structural engineering problems, and although the emergence of design codes is a step forward, their inefficiency (due largely to overly-simplistic material modelling) is inhibiting more widespread use.

It is clear that for a material with high initial cost, efficient design is paramount, and a more rigorous and complex design approach can be justified. A major laboratory testing programme has recently been completed at Imperial College London and the results from these tests have led to improved understanding of the structural behaviour of stainless steel and have formed part of the validation of a proposed new design procedure. Numerical modelling has also been used to extend the range of structural performance data and investigate the effects of systematic variation of key individual parameters. Full details of the laboratory testing and numerical modelling programmes have been described [1].

2.2 Overview of proposed design approach

The European, Australian/ New Zealand and North American structural stainless steel design codes place cross-sections into discrete behavioural classes on the basis of individual element slendernesses. A new design method has been developed that replaces these discrete classes by a single numerical value that is a measure of the deformation capacity of the cross-section. The deformation capacity is based upon slenderness of individual plate elements and the interaction between elements within the cross-section. Cross-section resistances are determined using a local buckling strength derived from the cross-section deformation capacity, in conjunction with an accurate material model appropriate for stainless steels. Member strengths are determined using the local buckling strength (raised to a power) in combination with overall buckling curves. Figure 1 shows a schematic representation of the design procedure, where b and t are internal element width and thickness respectively, A is cross-sectional area, W_{el} is elastic section modulus, $\sigma_{0.2}$ is the material 0.2% proof strength and E_0 is the material Young's modulus.

Full details of the development of the design method including worked examples have been reported by Gardner [1], and a concise presentation of the design method including a comparison with existing structural design codes has been prepared [2].

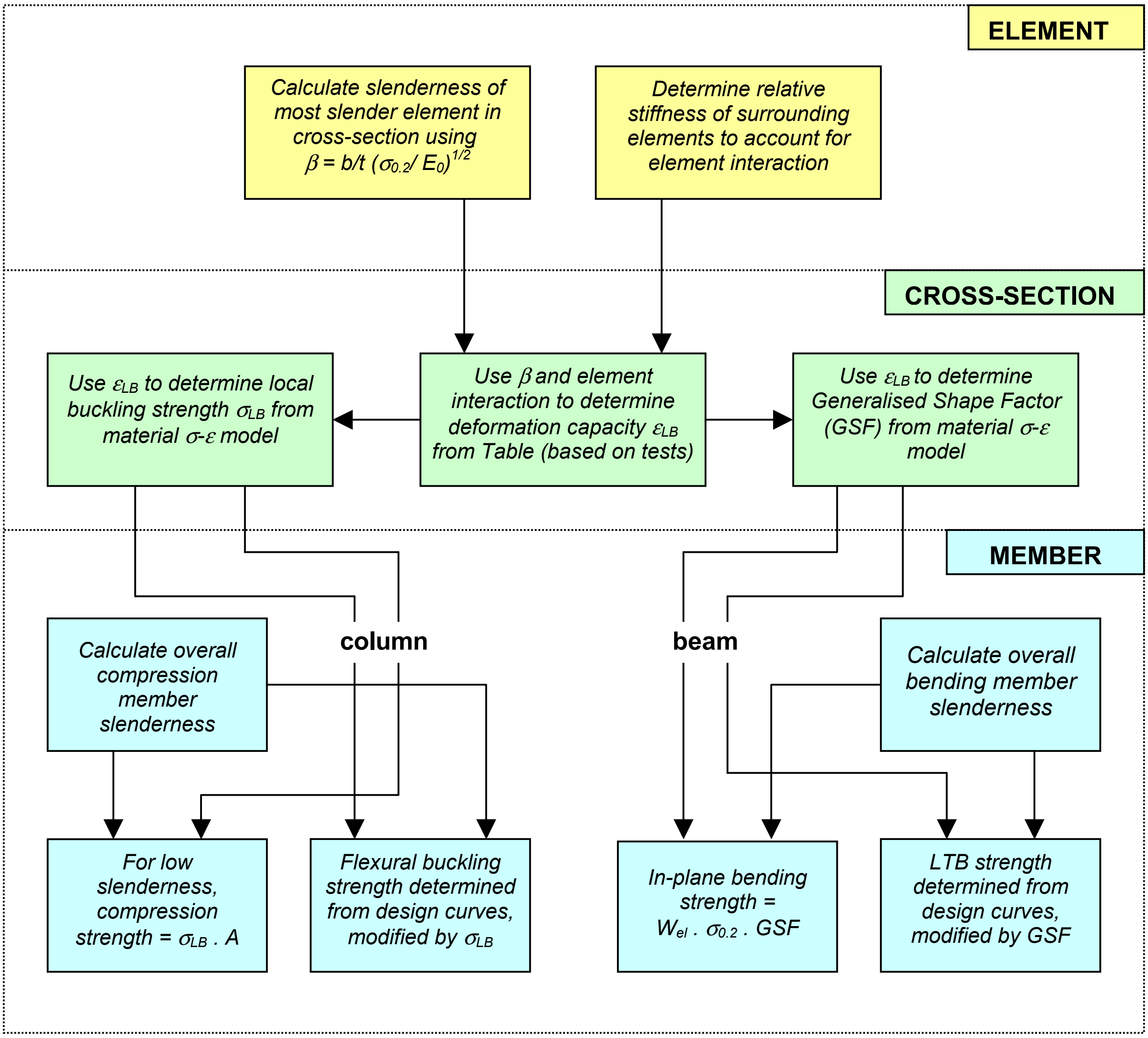

Figure 1 Schematic representation of design method

2.3 Design Method

Cross-section slenderness, β

Cross-section slenderness, β shall be determined for all internal elements from Equation 1 (for SHS & RHS) and Equation 2 (for CHS).

For SHS and RHS,
$$\beta = \left(\frac{b}{t}\right)\sqrt{\frac{\sigma_{0.2}}{E_0}}\sqrt{\frac{4.0}{k}} \quad (1)$$

For CHS,
$$\beta = \left(\frac{R}{t}\right)\left(\frac{\sigma_{0.2}}{E_0}\right) \quad (2)$$

where $\sigma_{0.2}$ is the material 0.2% proof stress in compression
E_0 is the material Young's modulus
b is the flat face width measured between centrelines of adjacent faces
R is the radius of the CHS measured to the centreline of the wall thickness
t is the wall thickness of the cross-section
k is the buckling coefficient from Table 1

Table 1 Buckling coefficients for compressed plate elements

$\psi = \sigma_1 / \sigma_2$	1	$1 > \psi > 0$	0	$0 > \psi > -1$	-1	$-1 > \psi > -2$
Buckling Coefficent, k	4.0	$\frac{8.2}{1.05 + \psi}$	7.81	$7.81 - 6.29\psi + 9.78\psi^2$	23.9	$5.98(1-\psi)^2$
Alternatively, for $1 \leq \psi \leq -1$: $k = \frac{16}{[(1+\psi)^2 + 0.112(1-\psi)^2]^{0.5} + (1+\psi)}$						

Note: ψ is the ratio of end stresses (compression positive) for the compression element

Cross-section deformation capacity, ε_{LB}

Based on β for the most slender element, cross-section deformation capacity, ε_{LB} may be determined from Equation 3 (SHS and RHS) or Equation 4 (CHS). For RHS subjected to pure compression only, allowance may be made for enhanced element edge restraint by taking χ equal to the aspect ratio of the cross-section. Strictly χ is the ratio of the stiffness of the longer face of the RHS to the stiffness of the shorter face, but for uniform material properties and thickness, this simplifies to the aspect ratio. For all other cases, χ should be taken as 1.0. Equations 3 and 4 were developed from the results of stub column tests [3].

SHS and RHS, $$\frac{\varepsilon_{LB}}{\varepsilon_0} = \frac{7.07}{\beta^{2.13+0.21\beta}} \chi^{-0.30\beta} \qquad (3)$$

CHS, $$\frac{\varepsilon_{LB}}{\varepsilon_0} = \frac{0.116}{\beta^{1.21+1.69\beta}} \qquad (4)$$

where χ is the cross-section aspect ratio for RHS subjected to pure compression and taken as 1.0 for all other cases
ε_0 is the elastic strain at the material compressive 0.2% proof stress = $\sigma_{0.2}/E_0$
ε_{LB} is the cross-section local buckling strain

Local buckling stress, σ_{LB}

Local buckling stress, σ_{LB} for any given local buckling strain, ε_{LB} is determined from Table 2 (SHS and RHS) or Table 3 (CHS), on the basis of a compound Ramberg-Osgood material model, described in [3].

Cross-section resistance - compression

Compression resistance, $N_{c,Rd}$, is given by Equation 5.

$$N_{c,Rd} = A\sigma_{LB} \qquad (5)$$

where A is the gross area of the cross section
σ_{LB} is the local buckling stress (from Table 2 or 3)

Table 2 Local buckling stress for SHS and RHS

$\sigma_{0.2}$ / ε_{LB}	σ_{LB} (N/mm^2)								
	200 N/mm^2	220 N/mm^2	240 N/mm^2	280 N/mm^2	320 N/mm^2	360 N/mm^2	400 N/mm^2	440 N/mm^2	480 N/mm^2
0.001	131	140	148	161	171	179	184	188	192
0.002	174	189	203	229	252	274	292	309	324
0.003	200	218	235	268	299	328	356	381	405
0.004	216	236	256	295	332	367	400	431	461
0.005	225	247	268	310	351	391	430	468	504
0.006	232	254	276	320	364	407	448	489	530
0.007	237	260	283	328	373	418	461	505	547
0.008	241	265	288	335	381	426	472	516	560
0.009	245	269	293	340	387	434	480	526	572
0.010	248	273	297	345	393	441	488	535	581
0.012	254	279	304	354	403	452	501	549	598
0.014	259	285	310	361	412	461	511	561	611
0.016	263	289	316	367	419	470	521	572	622
0.018	268	294	320	373	426	478	529	581	632
0.020	271	298	325	378	431	484	537	590	642
0.024	277	305	333	388	442	497	551	605	658
0.028	284	312	340	396	451	508	563	618	673
0.032	289	317	346	403	461	517	574	630	687
0.036	294	323	352	410	468	526	584	641	698
0.040	298	328	357	416	476	534	592	652	710
0.050	308	338	369	430	491	552	613	673	735
0.060	316	348	379	442	505	568	630	693	755
0.080	331	364	397	463	529	594	660	725	791
0.100	344	377	412	480	548	616	685	752	821

Table 3 Local buckling stress for CHS

$\sigma_{0.2}$ / ε_{LB}	σ_{LB} (N/mm^2)								
	200 N/mm^2	220 N/mm^2	240 N/mm^2	280 N/mm^2	320 N/mm^2	360 N/mm^2	400 N/mm^2	440 N/mm^2	480 N/mm^2
0.001	131	140	148	161	171	179	184	188	192
0.002	174	189	203	229	252	274	292	309	324
0.003	200	218	235	268	299	328	356	381	405
0.004	214	234	254	293	331	367	400	431	461
0.005	220	242	263	305	346	387	426	465	502
0.006	225	247	269	313	356	398	440	481	522
0.007	229	251	274	318	362	406	449	492	535
0.008	232	255	278	323	368	413	457	501	544
0.009	235	258	281	327	373	418	463	508	552
0.010	237	261	284	331	377	423	469	514	560
0.012	242	265	289	337	384	431	478	525	571
0.014	245	269	294	342	390	438	486	533	581
0.016	248	273	298	347	396	444	493	541	589
0.018	252	276	301	351	401	450	499	548	597
0.020	254	279	304	355	405	455	505	554	604
0.024	259	285	311	362	413	464	515	566	616
0.028	263	290	316	368	420	472	524	576	627
0.032	267	294	320	374	426	479	532	584	637
0.036	271	298	324	379	432	485	539	592	646
0.040	274	301	328	383	437	492	546	600	654
0.050	281	309	337	393	449	505	561	616	672
0.060	288	316	345	402	460	516	574	631	687
0.080	298	328	358	417	477	536	595	655	714
0.100	308	338	369	430	492	553	614	675	736

Cross-section resistance - bending
In-plane bending resistance, $M_{c,Rd}$, is given by Equation 6.

$$M_{c,Rd} = W_{el}\, \sigma_{0.2}\, a_g \tag{6}$$

where W_{el} is the elastic section modulus
a_g is the generalised shape factor (from Table 4 or 5 and Equation 7)

The generalised shape factor, a_g may be calculated using Equation 7, where the constants A_1 to A_4 may be determined from Table 4 for SHS and RHS and Table 5 for CHS. Tables 4 and 5 were produced by numerical integration of a compound Ramberg-Osgood material model through the cross-section depth.

$$a_g = A_1 + A_2\varepsilon_0 + A_3 a_p + A_4\varepsilon_0 a_p \tag{7}$$

where A_1 to A_4 are constants determined from Table 4 (SHS & RHS) and Table 5 (CHS)
a_p is the geometric shape factor of the cross-section

Cross-section resistance - combined compression and bending
Cross-sections subjected to combined compression and bending should satisfy Equation 8.

$$\frac{N_{Sd}}{\sigma_{LB}\, A} + \frac{M_{y,Sd}}{W_{el,y}\, \sigma_{0.2}\, a_{gy}} + \frac{M_{z,Sd}}{W_{el,z}\, \sigma_{0.2}\, a_{gz}} \leq 1 \tag{8}$$

where N_{Sd} is the applied axial compression
$M_{y,Sd}$ is the applied bending moment about the y-axis
$M_{z,Sd}$ is the applied bending moment about the z-axis
$W_{el,y}$ is the elastic modulus about the y-axis
$W_{el,z}$ is the elastic modulus about the z-axis
a_{gy} is the generalised shape factor about the y-axis
a_{gz} is the generalised shape factor about the z-axis

Buckling resistance - compression
Buckling resistances of SHS and RHS compression members and CHS compression members are given by Equations 9 and 10 respectively.

SHS and RHS, $$N_{b.Rd} = \chi A \sigma_{0.2} \left(\frac{\sigma_{LB}}{\sigma_{0.2}}\right)^{0.32} \tag{9}$$

CHS, $$N_{b.Rd} = \chi A \sigma_{0.2} \left(\frac{\sigma_{LB}}{\sigma_{0.2}}\right)^{0.80} \tag{10}$$

where χ is the buckling reduction factor given by Equation 11 (not limited to ≤ 1.0)

$$\chi = \frac{1}{\phi + [\phi^2 - \overline{\lambda}^2]^{0.5}} \tag{11}$$

where ϕ = $0.5[1 + \alpha(\overline{\lambda} - \overline{\lambda}_0) + \overline{\lambda}^2]$ is an imperfection factor (Table 6)
$\overline{\lambda}_0$ = is the limiting slenderness (Table 6)
$\overline{\lambda}$ = λ/λ_1
λ = L_E/i and is the slenderness for the relevant buckling mode
λ_1 = $\pi\, [E_0/\sigma_{0.2}]^{0.5}$
L_E is the effective column length
i is the radius of gyration about the relevant axis, found from properties of the gross cross-section

Table 4 Generalised shape factor calculation constants - SHS & RHS

ε_{LB}	A_1	A_2	A_3	A_4
0.0015	0.373	35.937	0.559	-193.75
0.0020	0.360	68.187	0.644	-207.92
0.0025	0.336	83.333	0.720	-206.67
0.0030	0.343	80.833	0.761	-193.33
0.0035	0.332	86.250	0.807	-187.50
0.0040	0.307	99.667	0.858	-188.33
0.0045	0.230	125.156	0.937	-196.87
0.0050	0.181	147.634	0.993	-203.31
0.0055	0.152	148.437	1.024	-193.75
0.0060	0.140	136.062	1.046	-175.42
0.0070	0.163	104.375	1.042	-137.50
0.0080	0.164	80.667	1.059	-110.00
0.0090	0.180	63.594	1.061	-90.63
0.0100	0.178	55.771	1.077	-79.58
0.0120	0.188	42.146	1.092	-62.08
0.0140	0.196	31.917	1.107	-50.00
0.0160	0.201	27.083	1.122	-43.33
0.0180	0.207	24.229	1.135	-38.75
0.0200	0.220	18.542	1.141	-32.50
0.0240	0.224	17.854	1.168	-29.58
0.0280	0.238	12.250	1.183	-23.33
0.0320	0.247	11.187	1.199	-21.25
0.0360	0.253	10.042	1.214	-19.17
0.0400	0.261	8.625	1.229	-17.50
0.0500	0.287	4.375	1.253	-12.50
0.0600	0.297	5.625	1.282	-12.50
0.0700	0.310	6.250	1.307	-12.50
0.0800	0.327	3.281	1.324	-9.37
0.1000	0.357	0.312	1.356	-6.25

ε_{LB} is the cross-section local buckling strain
A_1 to A_4 are constants to be used in Equation 7

Table 5 Generalised shape factor calculation constants – CHS

ε_{LB}	A_1	A_2	A_3	A_4
0.0015	0.373	35.937	0.559	-193.75
0.0020	0.346	67.187	0.656	-206.25
0.0025	0.329	83.438	0.726	-206.25
0.0030	0.343	77.969	0.761	-190.62
0.0035	0.308	95.312	0.824	-193.75
0.0040	0.226	127.187	0.911	-206.25
0.0045	0.149	156.094	0.986	-215.62
0.0050	0.097	172.969	1.036	-215.62
0.0055	0.084	163.906	1.052	-196.87
0.0060	0.085	143.281	1.057	-171.87
0.0070	0.108	100.000	1.050	-125.00
0.0080	0.124	70.937	1.049	-93.75
0.0090	0.135	54.375	1.050	-75.00
0.0100	0.134	47.344	1.061	-65.62
0.0120	0.135	38.594	1.078	-53.12
0.0140	0.145	27.344	1.086	-40.62
0.0160	0.151	22.656	1.094	-34.37
0.0180	0.153	20.937	1.106	-31.25
0.0200	0.160	18.594	1.113	-28.12
0.0240	0.173	9.688	1.124	-18.75
0.0280	0.168	15.156	1.147	-21.87
0.0320	0.185	8.594	1.151	-15.63
0.0360	0.186	9.844	1.166	-15.62
0.0400	0.195	6.875	1.172	-12.50
0.0500	0.255	-42.188	1.154	31.25
0.0600	0.263	-37.969	1.177	28.13
0.0700	0.277	-37.969	1.192	28.12
0.0800	0.278	-33.750	1.215	25.00
0.1000	0.295	-29.531	1.243	21.88

ε_{LB} is the cross-section local buckling strain

A_1 to A_4 are constants to be used in Equation 7

Table 6 Parameters for flexural buckling curves

Cross-section type	α	$\overline{\lambda}_0$
Cold-formed SHS and RHS	0.70	0.44
Cold-formed CHS	0.50	-0.10

Buckling resistance - bending (LTB)
Clearly SHS, CHS and RHS (bending about the minor axis) are not affected by lateral torsional buckling, so member resistance may be taken as the cross-section in-plane bending resistance. No design guidance is given for lateral torsional buckling resistance of RHS beams (bending about the major axis) due to an absence of supporting test data.

Combined axial load plus bending
The buckling resistance of members subjected to combined axial load plus bending may be evaluated through Equation 12 (for SHS and RHS) and Equation 13 (for CHS). Since no design guidance is given for lateral torsional buckling, therefore the major axis bending component given in Equations 12 and 13 only applies to members not affected by lateral torsional buckling.

$$\frac{N_{Sd}}{\chi_{min}\,\sigma_{0.2}\,A(\sigma_{LB}/\sigma_{0.2})^{0.32}}+\frac{\kappa_y\,M_{y,Sd}}{W_{el,y}\,\sigma_{0.2}\,a_{gy}}+\frac{\kappa_z\,M_{z,Sd}}{W_{el,z}\,\sigma_{0.2}\,a_{gz}}\le 1 \qquad (12)$$

$$\frac{N_{Sd}}{\chi_{min}\,\sigma_{0.2}\,A(\sigma_{LB}/\sigma_{0.2})^{0.80}}+\frac{\kappa_y\,M_{y,Sd}}{W_{el,y}\,\sigma_{0.2}\,a_{gy}}+\frac{\kappa_z\,M_{z,Sd}}{W_{el,z}\,\sigma_{0.2}\,a_{gz}}\le 1 \qquad (13)$$

where χ_{min} is the lesser of the buckling reduction factors χ_y and χ_z
κ_y is defined by Equation 14
κ_z is defined by Equation 16

$$\kappa_y = 1-\frac{\mu_y N_{Sd}}{N_{b,Rd,y}} \quad \text{but } \kappa_y \le 1.5 \qquad (14)$$

$$\mu_y = \overline{\lambda}_y(2\beta_{My}-4) + (a_{gy}-1) \quad \text{but } \mu_y \le 0.90 \qquad (15)$$

$$\kappa_z = 1-\frac{\mu_z N_{Sd}}{N_{b,Rd,z}} \quad \text{but } \kappa_z \le 1.5 \qquad (16)$$

$$\mu_z = \overline{\lambda}_z(2\beta_{Mz}-4) + (a_{gz}-1) \quad \text{but } \mu_z \le 0.90 \qquad (17)$$

β_{My} is the equivalent uniform moment factor from Table 7.

Table 7 is a reproduction of part of Figure 5.5.3 from ENV 1993-1-1 [4], providing equivalent uniform moment factors for common load cases.

Table 7 Equivalent uniform moment factors

Moment diagram	Equivalent uniform moment factor, β_M
End moments M_1 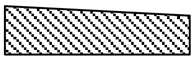 ψM_1 $-1 \leq \psi \leq 1$	$\beta_{M,\psi} = 1.8 - 0.7\psi$
Moments due to in-plane lateral loads 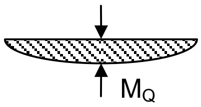 M_Q	$\beta_{M,Q} = 1.3$
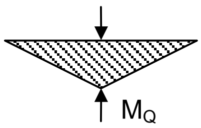 M_Q	$\beta_{M,Q} = 1.4$

M_1 is the applied end bending moment

M_Q is the applied mid-span bending moment

ψ is the ratio of the smaller end moment to the larger end moment

$\beta_{M,\psi}$ is the equivalent uniform moment factor for end moments

$\beta_{M,Q}$ is the equivalent uniform moment factor for moments due to in-plane lateral loads

2.4 Verification of proposed method

The purpose of this section is to analyse all available test data, compiled by Gardner [1] and to compare test failure loads and moments with those predicted by the current European [5], Australia/ New Zealand [6] and North American [7] stainless steel design codes and by the proposed design method. Tests were conducted in North America [8], Australia [9], Finland [10], Spain [11], Singapore [12,13,14] and recently at Imperial College London [1,15,16]. For comparison purposes, measured geometric and material properties are adopted, and all safety factors and load factors are set to unity. Where the design codes offer two methods for calculating resistances, the more favourable result is taken. Lateral torsional buckling rules have not been developed due to an absence of suitable test results, though this phenomenon is rarely encountered with hollow sections.

Cross-section resistance- compression

Table 8 presents a comparison between predicted results from the four considered design methods and test results for cross-sections in compression. A graphical illustration of the comparisons is given in Figure 2.

Table 8 Summary of comparison between predicted results and test results for cross-section compression resistance

Cross-section type	Predicted/Test Compression resistance for 4 design methods			
	Eurocode	**ASCE**	**AUS/ NZ**	**Proposed**
SHS & RHS MEAN:	0.78	0.78	0.78	0.95
SHS & RHS ST DEV:	0.13	0.13	0.13	0.08
CHS MEAN:	0.80	0.83	0.86	1.01
CHS ST DEV:	0.07	0.04	0.06	0.05
OVERALL MEAN:	**0.78**	**0.78**	**0.79**	**0.95**
OVERALL ST DEV:	**0.12**	**0.12**	**0.13**	**0.06**

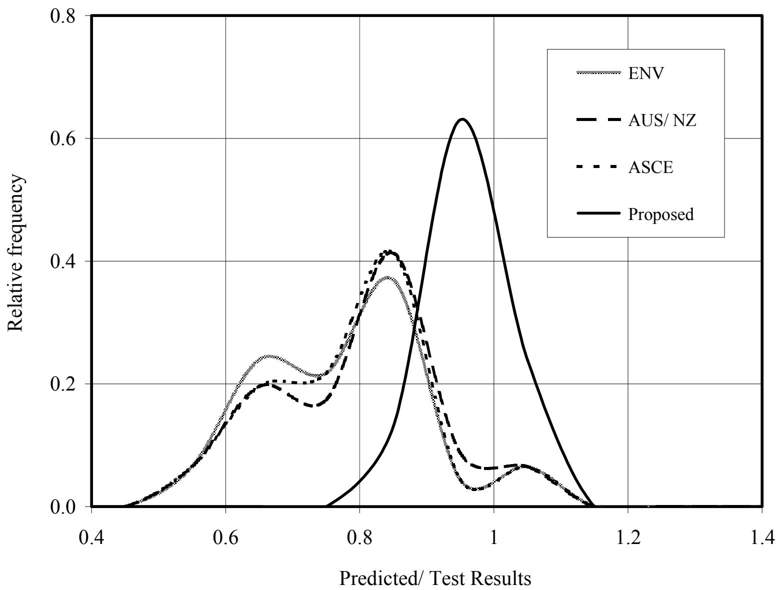

Figure 2 Graphical comparison between predicted results and test results for cross-section compression resistance (48 tests)

Cross-section resistance- bending

Table 9 and Figure 3 present a comparison between the results predicted by the four considered design methods and the test results for cross-sections subject to in-plane bending. It should be noted that ENV 1993-1-4 contains no guidance on the calculation of effective areas or effective moduli for Class 4 CHS. These are therefore calculated using the expressions provided in BS 5950: Part 1 [17].

Buckling resistance - compression

Table 10 and Figure 4 present a comparison between the buckling loads predicted by the four considered design methods and the test buckling loads. It should be noted that for pin-ended columns, effective lengths have been taken as the actual length, and for fixed-ended columns, effective lengths have been taken as 0.5 times the actual length.

Table 9 Summary of comparison between predicted results and test results for in-plane bending resistance

Cross-section type	Predicted/Test bending resistance for 4 design methods			
	Eurocode	**ASCE**	**AUS/ NZ**	**Proposed**
SHS & RHS MEAN:	0.69	0.72	0.74	0.92
SHS & RHS ST DEV:	0.06	0.08	0.08	0.08
CHS MEAN:	0.79	0.62	0.78	0.98
CHS ST DEV:	0.10	0.08	0.11	0.08
OVERALL MEAN:	**0.71**	**0.69**	**0.74**	**0.94**
OVERALL ST DEV:	**0.08**	**0.09**	**0.09**	**0.08**

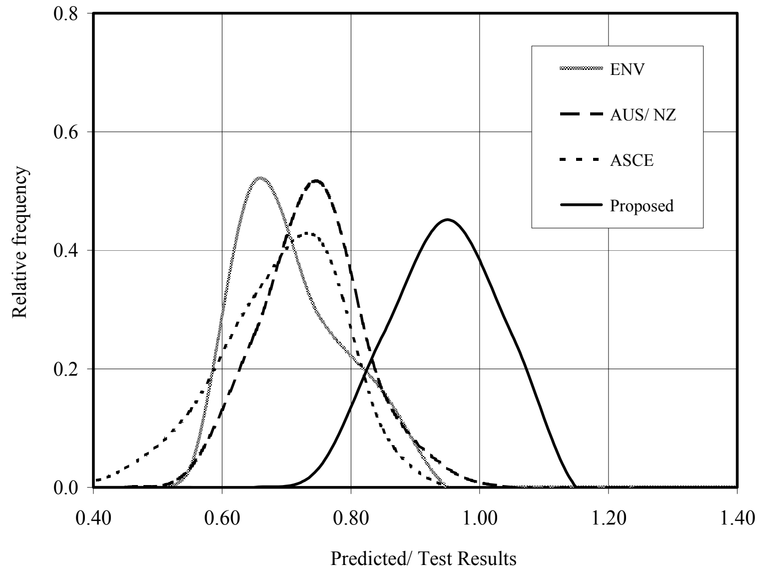

Figure 3 Graphical comparison between predicted results and test results for cross-section in-plane bending resistance (31 tests)

Table 10 Summary of comparison between predicted results and test results for flexural buckling resistance

Cross-section type	Predicted/Test buckling resistance for 4 design methods			
	Eurocode	**ASCE**	**AUS/ NZ**	**Proposed**
SHS & RHS MEAN:	0.91	0.95	0.95	1.00
SHS & RHS ST DEV:	0.14	0.15	0.15	0.10
CHS MEAN:	1.02	1.00	1.01	1.00
CHS ST DEV:	0.09	0.06	0.07	0.05
OVERALL MEAN:	**0.94**	**0.97**	**0.97**	**1.00**
OVERALL ST DEV:	**0.14**	**0.14**	**0.14**	**0.09**

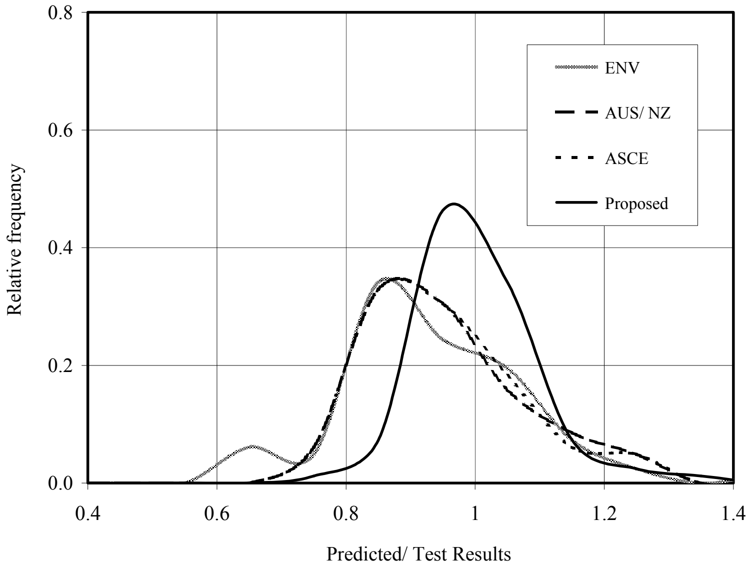

Figure 4 Graphical comparison between predicted results and test results for member flexural buckling resistance (82 tests)

Combined compression plus bending

Tests on eccentrically loaded pin-ended columns were conducted by Talja & Salmi [10]. The members were proportioned such that overall flexural buckling was the primary failure mode. These test results are therefore compared to the buckling resistances predicted by the four considered design methods. The comparisons are shown in Table 11 and Figure 5. No account for the possibility of lateral torsional buckling has been made, though no such effects were observed in the tests.

Table 11 Summary of comparison between predicted results and test results for beam-column buckling resistance

Cross-section type	**Predicted/Test beam-column resistance for 4 design methods**			
	Eurocode	**ASCE**	**AUS/ NZ**	**Proposed**
SHS & RHS MEAN:	0.77	0.81	0.82	0.98
SHS & RHS ST DEV:	0.15	0.13	0.13	0.12
CHS MEAN:	0.79	0.78	0.83	0.94
CHS ST DEV:	0.12	0.11	0.11	0.08
OVERALL MEAN:	**0.77**	**0.80**	**0.82**	**0.96**
OVERALL ST DEV:	**0.13**	**0.12**	**0.12**	**0.10**

2.5 Discussion

For cross-sections in compression and in bending and for members subjected to combined compression plus bending, the proposed design method provides approximately 25% higher resistances, whilst still delivering mean predicted/ test resistances of less than 1.0. For flexural buckling, which is governed predominantly by member instability, the improvement is smaller. In all cases scatter is reduced. Predictions for the three existing design codes are generally similar, which is unsurprising since their basis and approach are essentially the same. Results from the comparisons demonstrate the improved accuracy, economy and reliability of the proposals.

It is worth noting that for cross-sections in bending containing very slender plate elements, an effective width approach (adopted in all of the three considered current design codes) may provide more favourable results than the proposed method. The proposed method could be modified to adopt a similar approach for such elements, but it would of course necessitate the iterative calculation of a shift in neutral axis associated with Class 4 sections in bending.

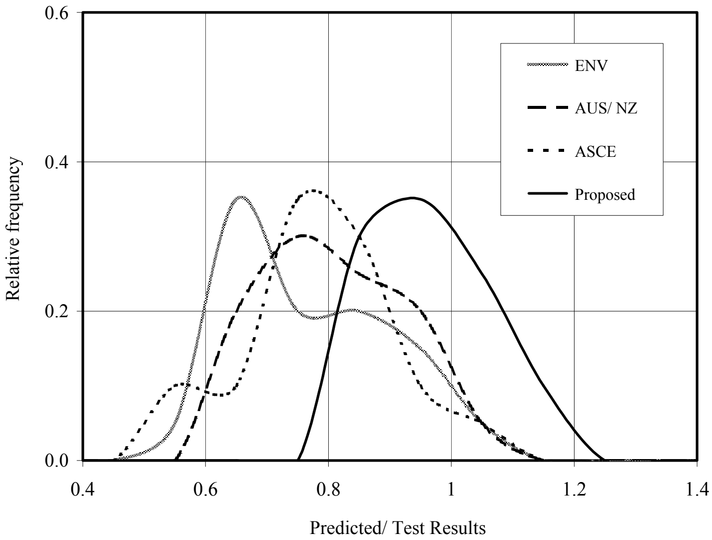

Figure 5 Graphical comparison between predicted results and test results for beam-column buckling resistance (20 tests)

3 FE MODELLING OF HIGH-STRENGTH STAINLESS STEEL COMPONENTS

3.1 Introduction

This section describes the numerical modelling of high strength stainless steel hollow sections. Initial analyses were conducted to simulate experimental tests [22] on 12 pin-ended columns, 6 simply supported beams proportioned to failure by flexure and 6 simply supported beams proportioned to fail at the internal support. Further studies were conducted to investigate the sensitivity of the models to variations in key parameters, and following successful replication of the experiments, parametric studies were performed to provide additional results. The general-purpose finite element (FE) software package ABAQUS [18] was employed throughout the study.

3.2 Modelling parameters

The elements chosen for the stub column models were 9-noded, reduced integration shell elements with five degrees of freedom per node, designated as S9R5 in the ABAQUS element library. This element has been shown to perform well in similar applications involving the modelling of stainless steel SHS and RHS flexural members [19], the local and global buckling of stainless steel SHS, RHS and CHS columns [1] and the buckling response of mild steel and high performance steel box columns in axial compression [20]. S9R5 is characterised as a 'thin' shell element and is not recommended for modelling cases where transverse shear flexibility is important. Transverse shear flexibility is said to become important when the shell thickness is more than about 1/15 of a characteristic length on its surface [18].

The curved geometry at the corners of the cross-sections was modelled using curved S9R5 shell elements. Convergence studies were conducted to decide upon an appropriate mesh density, with the aim of achieving suitably accurate results whilst minimising computational time. For the modelling of flexural buckling, linear elastic eigenmode simulations were conducted to provide buckling modes to be used as initial imperfections in subsequent non-linear analyses. The modified Riks method [18] was employed to solve the geometrically and materially non-linear stub column models. The modified Riks method is an algorithm that enables effective solutions to be found to unstable problems (e.g. post-ultimate response of compression or flexural members), and adequately traces non-linear unloading paths.

ABAQUS requires that material behaviour be specified by means of a multi-linear stress-strain curve, defined in terms of true stress and log plastic strain. Points to define this multi-linear stress-strain curve were taken from a compound two-stage Ramberg-Osgood material model fitted to the measured stress-strain data from tensile and compression tests. The concept of adopting a two-stage model was originally devised by Mirambell and Real [11]. A more complete description is provided by Gardner [1] and further analysis was carried out by Rasmussen [21].

Residual stresses are induced into cold-formed stainless steel hollow sections by deformations during the forming process and by non-uniform cooling following welding. The deformationally induced residual stresses (largely resulting in through-thickness bending) are also present in the material coupons. The effects of these are therefore inherently present. No residual stress measurements were taken during the present study, though previous FE simulations [1] have indicated that the effects of weld-induced residual stresses on cold-formed stainless steel tubular members is relatively small. A simple assumed residual stress pattern (with $\sigma_{0.2}$ in tension acting on a central portion, plate width, B/5 and an equilibrating compressive stress of $\sigma_{0.2}/4$ over the remainder of the plate) was adopted in all flexural buckling models. No residual stresses were specified in the bending or internal support tests.

Both local and global initial geometric imperfections were specified in the flexural buckling FE models. Since column flexural buckling behaviour is bifurcative, the presence of imperfections is important, and the sensitivity of models to the level of imperfection can be high. For the bending and internal support tests, failure is in the plane of the loading. These models are therefore less sensitive to imperfections and hence they have been excluded from these models. Local imperfections in the web of the internal support specimens could significantly effect its behaviour. Good agreement between test and FE results with no imperfections implies that the actual level of imperfection in the specimens was small.

For the flexural buckling models, the shapes of the local and global imperfections have been taken from an elastic eigenmode analysis. The lowest local eigenmode has been used for the shape of the local plate imperfection and the lowest global eigenmode has been used of the shape of the global imperfection.

The magnitude of the local imperfections have been taken from a study reported by Gardner [1] where the magnitude is defined in terms of the material and geometric properties of the plate elements, given by Equation 18. The global imperfection magnitude has been taken as the column length divided by 2000 (i.e. L/2000). A brief study is described in a later section to assess the sensitivity of the columns to variation in global imperfection amplitude.

$$\omega_0 / t = 0.023(\sigma_{0.2} / \sigma_{cr}) \qquad (18)$$

where ω_0 is the magnitude of the initial imperfection, t is the plate thickness, $\sigma_{0.2}$ is the material 0.2% proof stress and σ_{cr} is the critical buckling stress of the plate, assuming simply supported boundary conditions.

3.3 Comparison between test and FE results

This section compares the key results from the tests with those generated by FE modelling. The results are presented by test type in the following sub-sections: flexural buckling tests; bending tests; and internal support tests.

Flexural buckling tests

A total of twelve flexural buckling tests were conducted as part of the experimental study. Each of these tests was modelled using the described parameters above and a comparison between the test and FE results is presented in Table 12.

The results indicate that on average the FE models predict failure loads 1% higher than the test failure loads, and upon examination of the individual results it can be seen that the scatter is relatively small. I may therefore be concluded that FE modelling parameters found to be suitable for normal strength stainless steel sections are also applicable to the higher strength (cold-worked) sections. A study is conducted in the next section to assess the sensitivity of column buckling FE models to variation in global imperfection amplitude, and parametric studies are carried out to extend the range of results over a wider range of column non-dimensional slenderness.

In all cases the FE failure mode and the general form of the load-lateral deflection curves was similar to those observed in the tests. A comparison of test and FE load-lateral deflection response for the 100x100x3-C700 (length = 3546 mm) column is shown in Figure 6.

Table 12 Comparison between test and FE results for flexural buckling specimens

Cross-section	Length (mm)	Test failure load (kN)	FE Failure load (kN)	FE/ Test
RHS 80x80x3-C700	1148	407	423	1.04
RHS 80x80x3-C700	1850	267	293	1.10
RHS 80x80x3-C700	2849	150	172	1.15
RHS 80x80x3-C850	1147	518	512	0.99
RHS 80x80x3-C850	1847	332	332	1.00
RHS 80x80x3-C850	2848	162	175	1.08
RHS 100x100x3-C700	1447	560	492	0.88
RHS 100x100x3-C700	2250	406	377	0.93
RHS 100x100x3-C700	3546	220	229	1.04
RHS 100x100x3-C850	1447	634	571	0.90
RHS 100x100x3-C850	2250	427	418	0.98
RHS 100x100x3-C850	3552	222	227	1.02
MEAN:				**1.01**

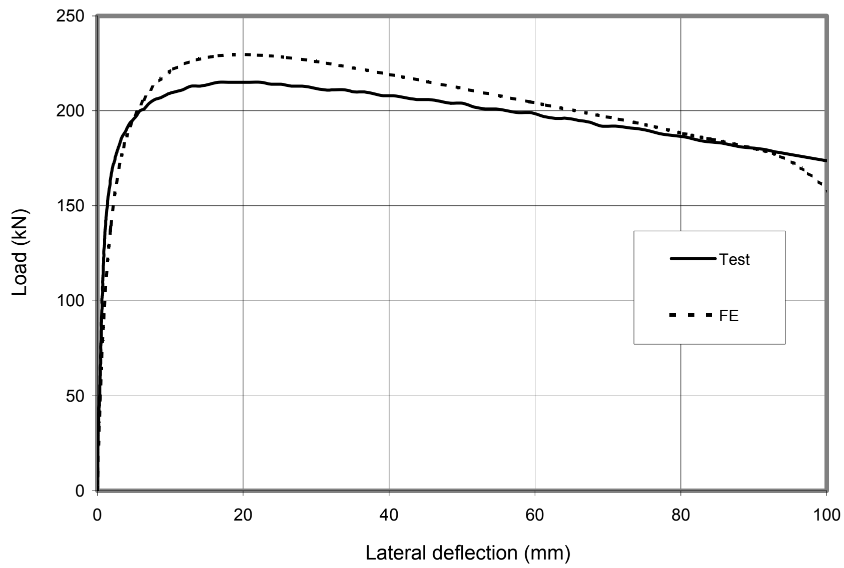

Figure 6 Comparison of test and FE load-lateral deflection response for 100x100x3-C700 (length = 3546 mm) column

Bending tests
A total of six bending tests were conducted as part of the experimental study. Each of these tests was modelled using the described parameters above and a comparison between the test and FE results is presented in Table 13.

Table 13 Comparison between test and FE results for bending specimens

Cross-section	Test failure moment (kNm)	FE failure moment (kNm)	FE/ Test
RHS 100x100x3-C700	23.3	21.0	0.90
RHS 120x80x3-C700	29.8	27.7	0.93
RHS 140x60x3-C700	34.6	30.0	0.87
RHS 100x100x3-C850	26.7	25.0	0.93
RHS 120x80x3-C850	33.7	32.8	0.97
RHS 140x60x3-C850	39.0	34.3	0.88
MEAN:			**0.91**

Table 13 shows that the FE prediction of the bending moment at failure is, on average, 9% lower than the test failure bending moment. It also shows that there is good consistency between the results. An explanation for the general under-prediction of strength by the FE model lies in the distribution of material properties around the cross-sections. This matter is analysed in the next section.

Figure 7 shows a deformed FE model of the RHS 120x80x3-C700 simply-supported beam. In the test arrangement, wooden blocks were positioned inside the bending specimens at the loading points and at the supports to avoid local crippling of the webs. This was modelled by constraining the out-of-plane deformation of the webs (to a common value) in these regions, though from Figure 7 some web deformation beneath the points of load application is still evident at large deflections. Only half of the cross-section for the bending and internal support specimens was modelled and symmetry boundary conditions applied.

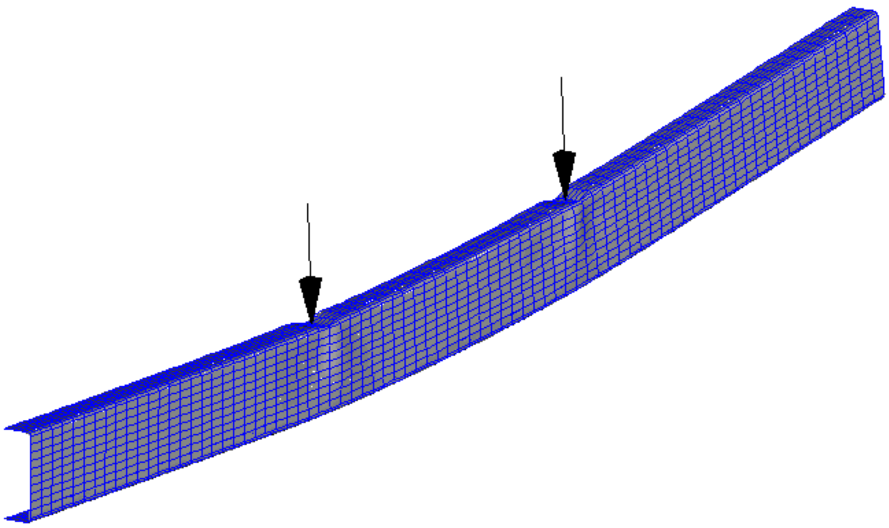

Figure 7 Deformed FE model of the RHS 120x80x3-C700 simply-supported beam

The general form of the test and FE bending moment versus vertical deflection at mid-span curves were similar in all cases. Some variation in the deflection at ultimate moment was observed, but this would be expected since the slope of the curve is low in this region. A typical comparison between test and FE bending moment versus vertical deflection at mid-span is shown for the RHS 120x80x3-C850 beam specimen in Figure 8.

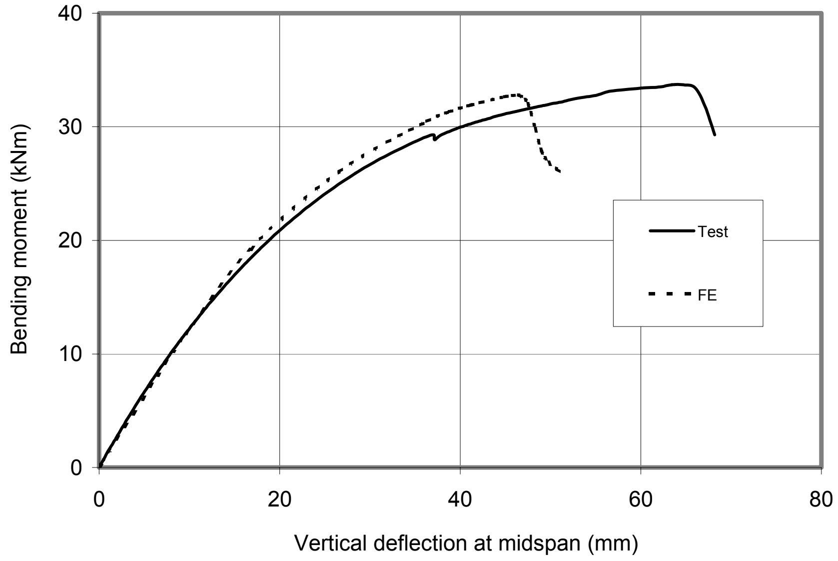

Figure 8 Comparison of test and FE bending moment versus vertical deflection at mid-span curve for RHS 120x80x3- C850 bending specimen

Internal support tests

Table 14 presents a comparison between the test and FE results for the six internal support test specimens.

Table 14 Comparison between test and FE results for internal support specimens

Cross-section	Test failure load (kN)	FE failure load (kN)	FE/ Test
RHS 100x100x3-C700	107.1	110.4	1.03
RHS 120x80x3-C700	108.3	102.6	0.95
RHS 140x60x3-C700	107.5	98.4	0.92
RHS 100x100x3-C850	119.2	119.2	1.00
RHS 120x80x3-C850	118.2	117.0	0.99
RHS 140x60x3-C850	126.7	112.2	0.89
MEAN:			**0.96**

The results demonstrate very good agreement in terms of magnitude of failure load with a mean value of FE failure load divided by test failure load of 0.96, and there is little scatter in the results.

Figure 9 shows a deformed FE model of the RHS 100x80x3-C700 internal support specimen. In the test arrangement, wooden blocks were positioned inside the cross-sections at the supports to avoid local crippling of the webs, but not under the point of load application. This was modelled by constraining the out-of-plane deformation of the webs at the supports, whilst providing no constraint to web in the region of load application. The load was introduced into each test specimen through a 50 mm wide steel plate. This was modelled by constraining a 50 mm width of the loaded flange to displacement vertically in unison. The failure mode of the FE model was of a similar shape to that observed in the tests.

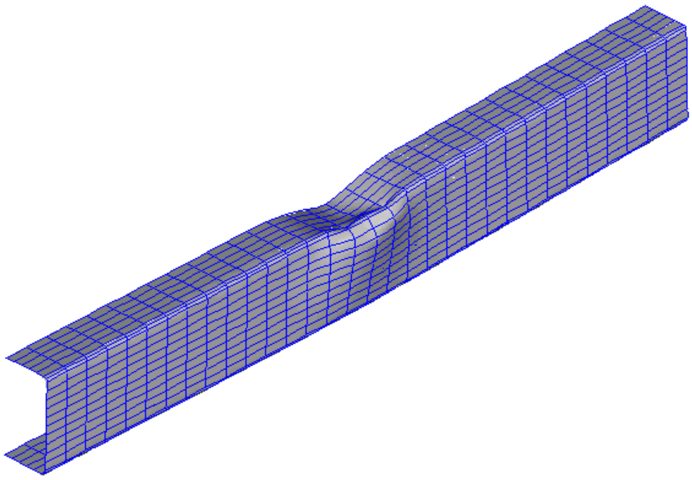

Figure 9 Deformed RHS 100x100x3 internal support specimen

3.4 Sensitivity and parametric studies

A series of sensitivity studies were conducted to investigate the response of the FE models to changes in key parameters.

Global imperfection amplitude

Although there is good overall agreement between test and FE results, comparing the test and FE behaviour of the flexural buckling members it can be seen that the strength of the most slender columns is generally over-predicted and the strength of the least slender columns is generally under-predicted. Sensitivity of the models to an increase in global imperfection amplitude was assessed. For the three RHS 80x80x3-C700 members, buckling loads for FE models with global imperfections of L/2000 (as above) and L/1000 are presented in Table 15.

Table 15 Sensitivity of column FE models to variation in global imperfection amplitude

Cross-section	Length (mm)	FE Failure load for L/2000 (kN)	FE failure load for L/1000 (kN)	Reduction in failure load (%)
RHS 80x80x3-C700	1148	423	411	2.8
RHS 80x80x3-C700	1850	293	282	3.8
RHS 80x80x3-C700	2849	172	163	5.2
MEAN:				**3.9**

The increase in FE global imperfection magnitude from L/2000 to L/1000 resulted in a mean reduction in buckling load for the three RHS 80x80x3-C700 columns of 3.9%. This represents relatively load imperfection sensitivity and as a general parameter it seems that a global imperfection magnitude of L/2000 is more appropriate.

Distribution of material properties

The results show that although the predicted (FE) bending strength is reliable (in the sense that there is little variability in FE/test results), the FE results are consistently lower than the corresponding test results. An explanation for this may lie in the distribution of material strength around the cross-section. It is clear that the bending specimens, where the extreme fibres in the flanges are far more highly stressed than the web regions, are likely to be more sensitive to variation in material distribution than the compressed specimens where the cross-sections are more uniformly loaded.

For the comparison between FE and test results given in the section above, average material properties have been uniformly distributed around the cross-sections, with the exception of the corner regions where enhanced strengths have been specified. For this study, material properties measured from the narrow faces will be applied to the two narrow faces of the cross-section and those measured from the wide faces will be applied to the two wide faces of the cross-section. It should be noted that the welds always appear on one of the two narrow faces and the test specimens were configured such that the weld was positioned on the underside of specimens; therefore for the square cross-sections, the material properties from the welded and opposite faces were applied to the extreme faces in tension and compression. The results are shown in Table 16.

Table 16 Bending FE models with uniform and distributed material properties

Cross-section	Test failure moment (kNm)	FE (uniform properties)/ Test failure moment (kNm)	FE (distributed properties)/ Test failure moment (kNm)
RHS 100x100x3-C700	23.3	0.90	0.99
RHS 120x80x3-C700	29.8	0.93	0.97
RHS 140x60x3-C700	34.6	0.87	0.89
RHS 100x100x3-C850	26.7	0.93	1.01
RHS 120x80x3-C850	33.7	0.97	0.99
RHS 140x60x3-C850	39.0	0.88	0.90
MEAN:		**0.91**	**0.96**

Table 16 indicates that more accurate distribution of material properties around the cross-section of the FE models leads to closer agreement with the test results. It is often the case that only one material test is conducted for each member. However, where detailed material property data is available, based on the findings of this study, it is recommended that properties be applied to the specific face from which measurements were taken.

Following the satisfactory agreement between test and FE model behaviour, a series of parametric studies, intended to generate a greater pool of results upon which design guidance may be based were conducted. Full details of the generated results were reported by Gardner and Talja [22].

3.5 Comparison with existing design guidance

This section presents a comparison of the test results with existing design rules from ENV 1993-1-4 [5] and the design rules proposed by Gardner and Nethercot [1] As with the FE modelling, comparison has been made according to test type in the following three sections: flexural buckling, bending and web crippling. Values from the two design methods have been generated using measured geometry and measured (weighted average) tensile material properties. All partial safety factors have been set to unity to enable a direct comparison.

Flexural buckling tests

Comparison between the flexural buckling test results and the results predicted by the two considered design methods is given in Table 17. The flexural buckling resistance according to the Eurocode method is described below. The flexural buckling resistance according to the Gardner/ Nethercot approach is described by Gardner [1].

The resistance to flexural buckling is determined from:

$$N_{\mathrm{b,Rd}} = \chi \, \beta_{\mathrm{A}} \, A_{\mathrm{g}} \, f_{\mathrm{y}} \, / \, \gamma_{\mathrm{M1}} \qquad (2)$$

where:

β_{A} = 1 for Class 1, 2, 3 cross-sections
= $A_{\mathrm{eff}}/A_{\mathrm{g}}$ for Class 4 cross-sections
A_{eff} is the effective area of Class 4 cross-section
A_{g} is the gross area

χ is the reduction factor accounting for buckling, given by:
γ_{M1} is set equal to unity for this comparison

$$\chi = \frac{1}{\varphi + \left[\varphi^2 - \overline{\lambda}^2\right]^{0,5}} \quad \leq \quad 1 \tag{3}$$

in which

$$\varphi = 0,5\left(1 + \alpha\left(\overline{\lambda} - \overline{\lambda}_0\right) + \overline{\lambda}^2\right) \tag{4}$$

$$\overline{\lambda} = \frac{l}{i}\frac{1}{\pi}\sqrt{\frac{f_y \beta_A}{E}} \tag{5}$$

where:

l is the buckling length (see below)
i is the radius of gyration of the gross cross-section
α is the imperfection factor taken as 0.49
$\overline{\lambda}_0$ is the limiting slenderness taken as 0.40

Table 17 Comparison between tests and design guidance for flexural buckling

Cross-section	$\sigma_{0.2}$ (N/mm^2)	E (N/mm^2)	Length (mm)	Test failure load (kN)	ENV / Test failure load	Gardner & Nethercot/ Test failure load
80x80x3-C700	520	187500	1148	407	1.01	1.05
80x80x3-C700	520	187500	1850	267	1.05	1.03
80x80x3-C700	520	187500	2849	150	1.01	0.99
80x80x3-C850	653	173000	1147	518	0.83	0.92
80x80x3-C850	653	173000	1847	332	0.82	0.85
80x80x3-C850	653	173000	2848	162	0.87	0.89
100x100x3-C700	487	195000	1447	560	0.78	0.90
100x100x3-C700	487	195000	2250	406	0.81	0.87
100x100x3-C700	487	195000	3546	220	0.82	0.86
100x100x3-C850	594	183500	1447	634	0.69	0.87
100x100x3-C850	594	183500	2250	427	0.73	0.83
100x100x3-C850	594	183500	3552	222	0.74	0.82
MEAN:					**0.85**	**0.91**

A graphical evaluation of the results against the ENV 1993-1-4 design curve is not straightforward because many of the cross-sections are class 4, which means there is not a single curve for comparison with.

Bending tests
Comparison between the bending test results and the results predicted by the two considered design methods are given in Table 18. Again, the Eurocode design expression are given below and those for the Gardner/ Nethercot method are reported by Gardner [1].

$$M_{b,Rd} \quad = \quad \chi_{LT}\, \beta_{W,y}\, W_{pl,y}\, f_y/\gamma_{M1} \tag{6}$$

where:

$\beta_{W,y}$ = 1 for Class 1 or 2 cross-sections
= $W_{el,y}/W_{pl,y}$ for Class 3 cross-sections
= $W_{eff,y}/W_{pl,y}$ for Class 4 cross-sections
$W_{pl,y}$ is the plastic modulus of cross-section about the major axis
$W_{el,y}$ is the elastic modulus of cross-section about the major axis
$W_{eff,y}$ is the elastic modulus of the effective section about the major axis
χ_{LT} is a reduction factor accounting for lateral torsional buckling, set equal to unity in this comparison since lateral torsional buckling does not occur ($\bar{\lambda}_{LT}$ < 0.4)
γ_{M1} is set equal to unity for this comparison

Table 18 Comparison between tests and design guidance for bending

Cross-section	$\sigma_{0.2}$ (N/mm^2)	E (N/mm^2)	Test failure moment (kNm)	ENV / Test failure moment	Gardner & Nethercot/ Test failure moment
100x100x3-C700	487	195000	23.3	0.71	0.86
120x80x3-C700	521	200000	29.8	0.68	0.93
140x60x3-C700	529	199100	34.6	0.62	1.00
100x100x3-C850	594	183500	26.7	0.72	0.84
120x80x3-C850	638	190400	33.7	0.73	0.97
140x60x3-C850	621	185600	39.0	0.64	1.00
MEAN:				**0.70**	**0.94**

Internal support tests
Comparison between the web crippling test results and the results predicted by the ENV 1993-1-4 are shown in Table 19. It should be noted that ENV 1993-1-4 refers the user to ENV 1993-1-3 [23] and this is therefore used as the basis for the comparison. The Gardner/ Nethercot design method has not been developed to cover web crippling.

ENV 1993-1-3 does not contain explicit rules for the determination of web crippling resistance for RHS. These sections are therefore dealt with assuming coefficients for sheeting – this is the same assumption made by Talja and Salmi [10]. Thus, for two webs, crippling resistance is given by Equation 11:

$$R_{\alpha,Rd} = 1.02t^2\sqrt{Ef_y}\,(1-0.1\sqrt{r/t})(0.5+\sqrt{0.02l_a/t})/\gamma_{M1} \qquad (7)$$

where:

t is the web thickness
r is the internal corner radii
E is the material Young's modulus
f_y is the material 0.2% proof strength
l_a is the length of the concentrated load
γ_{M1} is set equal to unity for this comparison

Table 19 Comparison between tests and design guidance for web crippling

Cross-section	$\sigma_{0.2}$ (N/mm^2)	E (N/mm^2)	Test failure load (kN)	ENV/ Test failure load
100x100x3-C700	487	195000	107.1	0.85
120x80x3-C700	521	200000	108.3	0.86
140x60x3-C700	529	199100	107.5	0.88
100x100x3-C850	594	183500	119.2	0.80
120x80x3-C850	638	190400	118.2	0.86
140x60x3-C850	621	185600	126.7	0.76
MEAN:				**0.83**

The comparison shows that the Eurocode predicts, on average, 83% of the failure load in web crippling, with a relatively small scatter. These results are approximately in line with those calculated by Talja and Salmi [10] for standard strength material.

3.6 Recommendations for design guidance

Comparison of the test results with the Eurocode design method and the method developed by Gardner and Nethercot has revealed similar predicted/ test ratios as were observed from an extensive comparison for standard strength stainless steel specimens [1].

Based on the recent testing programme on cold-worked structural stainless steel members, the Eurocode design rules that are currently limited to standard strengths of stainless steel may therefore safely be extended in scope to additionally cover high-strength cold-worked sections. The Gardner/ Nethercot design method demonstrates a similar level of improvement over the Eurocode approach through more accurate material modelling and section classification as for standard strength specimens.

3.7 Concluding remarks

The following concluding remarks can be made:

- Accurate replication of test behaviour for flexural buckling, bending and web crippling has been achieved using the FE package ABAQUS.
- Improved agreement between test and FE results was achieved by using face specific material properties rather than weighted average material properties on all faces.
- The Eurocode design rules have been shown to be equally applicable to high strength cold-worked stainless steel members as standard strength members.
- The Gardner/ Nethercot design approach has demonstrated similar improvements over the Eurocode method as for the standard strength material.

4 CONCLUSIONS

In this paper, a new design method for stainless steel hollow section structures loaded in compression, bending and combined compression plus bending has been presented. The approach has been validated against all available test results and compared with current structural stainless steel design codes.

In addition to the clear benefit in terms of enhanced strength prediction offered by the proposed design method (~25% overall), the reduction in scatter (standard deviation) of the prediction is also advantageous since design curves are typically 2-3 standard deviations below mean curves. The design method represents a considerable material and thus cost saving. It is envisaged that the proposed design method may be considered for incorporation into future revisions of Eurocode 3, bringing greater efficiency to structural stainless steel design and promoting more widespread use of the material.

Accurate replication of the behaviour of high-strength cold-worked stainless steel structural components has been achieved using the FE package ABAQUS. The Eurocode design method has been shown to be equally applicable to high strength stainless steel as to the standard grades, and the Gardner/ Nethercot design approach has demonstrated a similar level of improvement over the Eurocode approach as for standard strength material.

5 ACKNOWLEDGEMENTS

The researchers would like to thank ECSC, EPSRC and the AvestaPolarit UK Research Foundation for the funding the described projects. Work described in the first part of the paper was conducted under the supervision of Professor David Nethercot from Imperial College London and code comparisons were made with the assistance of Imma Estrada from the Universitat Politècnica de Catalunya. Technical advice was given by Nancy Baddoo from The Steel Construction Institute and David Dulieu from the AvestaPolarit UK Research Foundation.

6 REFERENCES

[1] Gardner, L. A new approach to stainless steel structural design. PhD Thesis. Structures Section, Department of Civil and Environmental Engineering, Imperial College, London. 2002.

[2] Gardner, L., Nethercot, D. A.. and Estrada, I. An efficient method for designing stainless steel structures. Proceedings of the Structural Stability Research Council Annual Technical Session and Meeting. Baltimore, USA. 2003.

[3] Gardner, L. and Nethercot, D. A. (submitted for publication). Experiments on stainless steel hollow sections – Part 1: Material and cross-sectional behaviour. Journal of Constructional Steel Research.

[4] ENV 1993-1-1. Eurocode 3: Design of steel structures – Part 1.1: General rules and rules for buildings. CEN. 1992.

[5] ENV 1993-1-4. Eurocode 3: Design of steel structures - Part 1.4: General rules - Supplementary rules for stainless steel, CEN. 1996.

[6] Aust/NZS. Cold-formed stainless steel structures. Australian/ New Zealand Standard AS/NZS 4673:2001. Sydney, Australia: Standards Australia. 2001.

[7] ASCE. Specification of the Design of Cold-Formed Stainless Steel Structural Members, ANSI/ASCE 8-90. American Society of Civil Engineers. New York. 1991.

[8] Johnson, A. L. and Winter, G. Behaviour of stainless steel columns and beams. Journal of the Structural Division, ASCE, ST5, 97-118, 1966.

[9] Rasmussen, K. J. R. and Hancock, G. J. Design of cold-formed stainless steel tubular members. I: Columns. Journal of Structural Engineering, ASCE, 119: 8, 2349-2367. 1993.

[10] Talja, A. and Salmi, P. Design of stainless steel RHS beams, columns and beam-columns. Research Note 1619, VTT Building Technology, Finland. 1995.

[11] Mirambell, E. and Real, E. On the calculation of deflections in structural stainless steel beams: an experimental and numerical investigation, Journal of Constructional Steel Research. 54, 109-133. 2000.

[12] Liu, Y. and Young, B. (2003). Buckling of stainless steel square hollow section compression members. Journal of Constructional Steel Research. 59:2, 165-177.

[13] Young, B. and Liu, Y. (2003). Experimental investigation of cold-formed stainless steel columns. Journal of Structural Engineering, ASCE. 129:2, 169-176.

[14] Young, B. and Hartono, W. (2002). Compression tests of stainless steel tubular members. Journal of Structural Engineering, ASCE. 128:6, 754-761.

[15] Gardner, L. and Nethercot, D. A. Tests on stainless steel structural hollow sections. Proceedings of the Structural Stability Research Council Annual Technical Session and Meeting. Baltimore, USA. 379-401. 2003.

[16] Gardner, L. and Nethercot, D. A. (submitted for publication). Experiments on stainless steel hollow section members – Part 2: Behaviour of columns and beams. Journal of Constructional Steel Research.

[17] BS 5950-1. Structural use of steelwork in buildings – Part 1: Code of practice for design in simple and continuous construction: hot rolled sections. British Standards Institution. 2000.

[18] ABAQUS. ABAQUS/ Standard User's Manual Volumes I-III and ABAQUS Post Manual. Version 6.3. Hibbitt, Karlsson & Sorensen, Inc. Pawtucket, USA. 2002.

[19] Real, E. Aportaciones al estudio del comportamiento a flexion de estructuras de acero inoxiddable. Tesis Doctoral. Departamento de Ingeniería de la Construcción, Universitat Politècnica de Catalunya. UPC-ETSECCP. Barcelona, Mayo. (In Spanish). 2001.

[20] Kiymaz, G. Stability criteria for thin-walled box columns of high performance steel in axial compression. PhD Thesis. Structures Section, Department of Civil Engineering, Imperial College, London. 1999.

[21] Rasmussen, K. J. R. Full range stress-strain curves for stainless steel alloys. Journal of Constructional Steel Research. 59, 47-61. 2003.

[22] Gardner, L. and Talja, A. WP2: Structural hollow sections. ECSC Project: Structural Design of Cold-Worked Austenitic Stainless Steel. Contract No. 7210 PR318. The Steel Construction Institute. 2003.

[23] ENV 1993-1-3. Eurocode 3: Design of steel structures – Part 1.3: General rules – Supplementary rules for cold formed thin gauge members and sheeting. CEN. 1996.